Article

Xc- System as a Possible Target for ConBr Lectin Interaction in Glioma Cells

Vanir Reis Pinto-Junior [1,2], Rodrigo Lopes Seeger [3], Cláudio Henrique Dahne Souza-Filho [3], Angela Patricia França [3], Nicole Sartori [3], Messias Vital Oliveira [1], Vinicius Jose Silva Osterne [1,4], Kyria Santiago Nascimento [1], Rodrigo Bainy Leal [3,*] and Benildo Sousa Cavada [1,*]

[1] Department of Biochemistry and Molecular Biology, BioMolLab, Federal University of Ceara, Fortaleza 60020-181, CE, Brazil; vanirjr.ufc@gmail.com (V.R.P.-J.); messiassigma@gmail.com (M.V.O.); vinnyosterne@gmail.com (V.J.S.O.); kyriasantiago@gmail.com (K.S.N.)
[2] Department of Physics, Federal University of Ceara, Fortaleza 60020-181, CE, Brazil
[3] Department of Biochemistry and Postgraduate Program in Biochemistry, Center for Biological Sciences, University Campus, Federal University of Santa Catarina, Florianópolis 88040-900, SC, Brazil; rlseeger@yahoo.com (R.L.S.); falecomclaudiodahne@gmail.com (C.H.D.S.-F.); angels_franca@hotmail.com (A.P.F.); nicolesartorigil@gmail.com (N.S.)
[4] Laboratory of Biochemistry and Glycobiology, Department of Biotechnology, Ghent University, 9000 Ghent, Belgium
*   Correspondence: rbleal@gmail.com (R.B.L.); bscavada@ufc.br (B.S.C.)

Abstract: Studies have revealed the dependence of glioma cells on iron, making them sensitive to ferroptosis. Ferroptosis can be triggered by inhibition of the xc- system, resulting in redox imbalance and membrane lipid peroxidation. The xc- system is composed of two coupled proteins, xCT and CD98hc. The control of transporters, such as xCT, by the CD98hc glycoprotein suggests that molecules targeting glycans may have an impact on the treatment of glioma. This study evaluated the effect of the *Canavalia brasiliensis* (ConBr) lectin on C6 glioma cells and compared it with erastin, an xc- system inhibitor. Both induced dose-dependent cell death, accompanied by an increase in the production of reactive oxygen species and a decrease in reduced glutathione. However, co-treatment did not show an additive effect. The analysis was updated by molecular dynamics assessments of the xc- system interacting with ConBr or erastin. The interaction of erastin with the xc- system affects its interaction with ConBr, reducing the antagonistic effect when both are in the protein complex. The data show that ConBr is effective in inducing cell death in glioma cells and regulates the xc system through interaction with CD98hc glycans, showing that lectins have the potential to promote ferroptosis in glioma cells.

Keywords: glioma; lectin; xc- system

1. Introduction

Primary tumors of the central nervous system (CNS), which include gliomas, embryonal tumors, and meningiomas, originate from the nervous system itself and are characterized by high morbidity and mortality [1,2]. Gliomas, despite representing around 30% of primary brain tumors, make up 80% of malignant tumors, being responsible for most deaths from primary brain neoplasms. Glioblastoma multiforme (GBM) is the most common and most aggressive type of glioma. GBM cells are characterized by being very infiltrative, with the ability to self-renew, and with characteristics of undifferentiated cells [2]. Furthermore, they present mechanisms of resistance to temozolomide (TMZ—the main chemotherapy drug of choice against GBM), as well as other chemotherapy drugs and radiotherapy [3,4]. In addition to changes in the expression and activity of several proteins involved in cell signaling, glioma cells present changes in the glycosylation pattern, which can activate signaling pathways involved in differentiation, intercellular and extracellular

matrix interactions, migration, invasion, and proliferation [5,6]. All these glioma characteristics, associated with the limited efficiency of available chemotherapy drugs and their side effects, make the clinical prognosis of GBM very unfavorable, with a mean survival of 14–16 months [2,7].

Lectins are proteins that specifically recognize and reversibly bind to glycans, whether in their free form or conjugated with proteins or lipids. This type of interaction between lectins and cell-surface glycoproteins or glycolipids can trigger numerous biological effects. In recent years, there has been an increasing number of studies on lectins obtained from plants and their properties for identifying and modulating specific cell types, with special emphasis on antitumor properties [8–12].

We have demonstrated the antiglioma activity of several lectins from leguminous plants with different degrees of potency and without apparent toxicity for the primary culture of astrocytes [13,14], suggesting a selective action of the lectins studied on tumor cells. The main activities include cytostatic effects, caspase activation, and stimulation of autophagy in C6 and U87 glioma cell lines. Therefore, the antiglioma potential of leguminous lectins has been demonstrated for Diocleinae subtribe including that purified from seeds of *Canavalia brasiliensis* (ConBr) [13], *Canavalia grandiflora* (ConGF) [14], *Dioclea lasiophylla* (DlyL) [15], *Dioclea violacea* (DvL) [16] and *Dioclea sclerocarpa* (DSL) [17].

Despite all these findings, specific lectin targets have yet to be well characterized, and this issue needs to be improved. Alteration of the glycosylation pattern in gliomas, as well as the secretion of certain glycoproteins, is recognized as favoring their ability to interact with the tumor microenvironment, as well as their response to the various signals that coordinate tumor proliferation and migration [5,6]. Within this paradigm, several glycoproteins have been identified as potential targets for the treatment of gliomas, including thrombospondin [18], metabotropic [19], and ionotropic (e.g., AMPA) glutamatergic receptors [20,21], and metalloproteinases [14,22,23].

The xc- system is a membrane antiporter amino acid transporter that performs cystine/glutamate exchange. It is composed of a light transmembrane subunit (xCT), also known as SLC7A11, responsible for transport, and a heavy subunit, represented by the glycoprotein CD98hc (also known SLC3A2; 4Fh2c) linked to xCT by one disulfide bond [24,25]. Hence, via the xc- system, cystine is incorporated into the intracellular environment, while glutamate is exported to the extracellular space. Cystine is then reduced to cysteine which will be used for the synthesis of glutathione (GSH)—the most abundant intracellular antioxidant [26,27]. This system is positively regulated in gliomas, and several studies have shown that its overexpression confers a tumor growth advantage [27]. This occurs both by increasing extracellular glutamate levels, which facilitates tumor expansion, and by increasing glutathione (GSH) production, which maintains redox potential and neutralizes reactive oxygen species (ROS) in the intracellular environment [28]. Importantly, GSH acts as a reducing agent to suppress ferroptosis, which is a consequence of ROS production and lipoperoxidation when the xc- system is inhibited [25,26,29,30]. Thus, the maintenance of intracellular GSH, as a ROS buffering mechanism, is essential for the survival, proliferation, and resistance of tumor cells [27,29,31].

Notably, the CD98hc (SLC3A2) regulatory subunit is highly glycosylated and, via interaction with the transmembrane xCT subunit, plays a role in the regulatory activity of the Xc-antiporter system [24,32–34]. Importantly, a recent study by Hasegawa et al. demonstrated that the glycans present in CD98hc can be altered in tumor cells, as they demonstrated that monoclonal antibodies directed against the CD98hc glycans of myeloma multiple cells promoted the selective death of the tumor cells [35].

Considering the antiglioma properties of legume lectins, as well as their ability to recognize certain glycans with high selectivity [36], in the present study we evaluate the capability of ConBr to modulate the xc- system. ConBr was demonstrated previously to act on C6 glioma cells, inhibiting cell migration and inducing cell death mainly via autophagy [13]. Hence, we perform a set of experiments to demonstrate the cytotoxic activity of ConBr on C6 glioma cells and measure reactive oxidant species (RS) production,

as well as the level of intracellular non-protein thiols (mainly glutathione) in response to ConBr. In addition, we compare the ConBr effects with erastin, a well-known xCT inhibitor that reduces intracellular glutathione, promoting lipid peroxidation and cell death by a mechanism known as ferroptosis [25,27,29,37]. Moreover, applying bioinformatics tools, we move to evaluate the plausibility that ConBr could modulate the xc- system via interaction with glycans present on the CD98hc regulatory subunit, using docking and molecular dynamics. Our data demonstrate the antiglioma activity of ConBr and indicate the potential of this lectin to inhibit the Xc-antiporter via CD98hc glycan interaction. As a consequence, by decreasing the level of GSH and elevating the level of RS, ConBr might promote glioma cell death, possibly via the ferroptosis mechanism.

2. Materials and Methods

2.1. Cell Culture of Rat Glioblastoma C6 and Treatment

C6 cells from Wistar rat (*Rattus norvegicus*) glioblastoma (ATCC-CCL-107) were obtained from the cell bank in Rio de Janeiro (Brazil). Cells were grown in culture bottles having 25 cm^2 of growth area with Dulbecco's Modified Eagle's Medium (DMEM) supplemented with 10% (*v/v*) fetal bovine serum (FBS) (Gibco$^®$, Waltham, MA, USA), 100 units/mL penicillin, and 100 mg/mL streptomycin (Gibco$^®$) at 37 °C in a humidified atmosphere of 95% air and 5% CO$_2$. The medium was changed every two days until the cells reached confluence. To carry out the experiments, cells were washed with phosphate-buffered saline (PBS) (140 mM NaCl, 3 mM KCl, 10 mM Na$_2$HPO$_4$, and 2 mM KH$_2$PO$_4$, pH 7.4) and chemically dissociated by trypsin. C6 cells were seeded in plates of 96-well with DMEM medium supplemented with 10% (*v/v*) FBS (Gibco$^®$), 100 units/mL penicillin, and 100 mg/mL streptomycin (Gibco$^®$) for 24 h at 37 °C in a humidified atmosphere of 95% air and 5% CO$_2$. Prior to treatments, the plates were observed under an inverted microscope to assess adherence and confluence. Hence, the culture media were replaced with fresh media containing vehicle or ConBr at concentrations of 5–100 μg/mL (as indicated in the figure legends) and incubated for 24 h. Alternatively, cells were treated with erastin (xCT inhibitor) at concentrations from 0.5 up to 50 μM (as indicated in the figure legends) and incubated for 24 h. For combined treatments, ConBr 30 μg/mL and erastin 10 μM were used for 24 h. The lectin was diluted with HEPES–saline buffer without glucose composed of NaCl 124 mM, KCl 4 mM, MgSO$_4$ 1.2 mM, HEPES 25 mM, and CaCl$_2$ 1 mM, pH 7.4. For all assays, the control cell cultures were incubated with a vehicle (HEPES–saline buffer without glucose). To evaluate whether the action of ConBr was dependent on its carbohydrate-recognition domain, ConBr was blocked (iConBr) by diluting the lectin in glucose-free HEPES-saline buffer containing 0.1 M of its specific binding sugar (α-methyl-D-mannoside) and maintained for 30 min at 37 °C before treating cells.

2.2. Cell Viability

Cell viability was estimated by MTT [30-(4,5-dimethylthiazol-2yl) 2,5-diphenyltetrazolium bromide] reduction assay as previously described by Mosmann [38]. Briefly, C6 glioma cells were seeded in 96-well plates at 10^4 cells/well and incubated for 24 h with the treatments. After treatments, the medium was removed, and cells were incubated for 1 h at 37 °C with 0.5 mg/mL MTT. Reduced MTT formazan crystals were dissolved with 100 mL dimethylsulfoxide (DMSO) for 30 min at 37 °C, and the absorbance was evaluated at 540 nm using a Tecan$^®$ (Männedorf, Switzerland) Microplate Reader Infinite M200 reader, equipment at the Laboratório Multiusuário de Estudos em Biologia at the Universidade Federal de Santa Catarina (LAMEB/UFSC). The results were expressed as a percentage of the control/vehicle group (considered as 100% viable).

2.3. Reactive Species Production

Reactive species (RS) production was evaluated by using the 2,7-dichlorodihydrofluorescein diacetate (H2DCF-DA, Sigma$^®$, Waltham, MA, USA) fluorescent probe. Briefly, C6 cells were plated in a 96-well plate at 10^4 cells/well for 24 h and then treated. The culture

medium was removed, and the cells were washed with PBS and incubated at 37 °C for 30 min with 10 μM H2DCF-DA. The H2DCF-DA solution was discarded, the cells were washed with PBS, and 100 mL PBS was added for fluorescence reading at 485/520 nm (excitation/emission) using a Tecan® Microplate Reader Infinite M200 reader, equipment at the Laboratório Multiusuário de Estudos em Biologia at the Universidade Federal de Santa Catarina (LAMEB/UFSC).

2.4. Non-Protein Thiol (NPSH) Content Quantification

GSH content was measured as non-protein thiols (NPSH) according to a method previously described (Ellman, 1959) [39]. C6 cells were seeded in 6-well plates at a density of 5×10^5 cells/well. Twenty-four hours after seeding, cells were exposed to the treatments for 24 h. After treatments, cells were rinsed and harvested in 150 mL of PBS-Triton buffer (PBS buffer pH 7.4 containing 0.05% Triton X-100) and mixed with 180 μL of 10% cold trichloroacetic acid (TCA), followed by centrifugation at $5000\times g$ for 10 min. After centrifugation, the supernatant was incubated with DTNB (10 mM), and the absorbance was measured at 412 nm using a Tecan® Microplate Reader Infinite M200 reader, equipment at the Laboratório Multiusuário de Estudos em Biologia at the Universidade Federal de Santa Catarina (LAMEB/UFSC). A GSH curve was used to calculate the NPSH content (nmol NPSH), and the data were expressed as a percentage of the control group.

2.5. Statistical Analysis

Four independent experiments were performed in triplicate, and the results were analyzed using GraphPad Prism version 5.0 (La Jolla, CA, USA). The data presented normal distribution according to the Shapiro–Wilk test ($p < 0.05$) and, therefore, were evaluated using Analysis of Variance (One-way ANOVA) followed by the Tukey post-hoc test. p values less than 0.05 ($p < 0.05$) were considered statistically significant.

2.6. Molecular Docking of ConBr with N-glycans Present in CD98hc and Construction of the ConBr-Xc- System Complex

Glycans have been selected based on the work of Powlesland et al. (2009) [40], which described the N-glycans present in the CD98hc protein using mass spectrometry.

Selected glycan structures were drawn using the GLYCAM-web server (https://glycam.org/, accessed on 1 August 2022), and their structures were minimized using the GLYCAM_06 force field [41]. The designed glycan structures have been applied in combination with the ConBr structure (PDB ID: 1AZD) [42] to perform molecular docking simulations. For this purpose, the GOLD v2023.2 software was used (CCDC, Cambridge, UK), with default settings. The simulation utilized the following parameters: a population size of 100, selection pressure of 1.1, number of operations of 10,000, number of islands of 5, niche size of 2, crossover frequency of 0.95, and number of poses of 100. The carbohydrate recognition domain of ConBr (CRD, centered around the amino acid Asp208) and all atoms in a 12 Å radius were defined as the application point of the program algorithm. The PLANTSPLP scoring function was used to calculate the docking score [43]. The best model was selected considering the combination of score values, hydrogen bonds, geometric penalties, and nonpolar interactions [44]. After docking between ConBr and the glycoconjugates individually, the one that showed the best interaction with the protein was chosen for the following steps.

The next step consisted of inserting glycans into the CD98hc (or 4F2hc) protein (PDB ID: 7EPZ) [44] in its four previously described glycosylation sites (365, 381, 424, and 506, based on the sequence of the Uniprot ID: P08195). The GlcNAc2-Man7 (MAN7) glycan was chosen to be inserted, as it demonstrated a good interaction with ConBr and, in addition, presented a good relative abundance among the other potential glycans for CD98hc [40]. Glycosylated CD98hc was prepared using the Glycoprotein builder tool of the GLYCAM-Web server (https://glycam.org/, accessed on 1 August 2022). Next, the ConBr monomer was coupled to the xc- system, more specifically to the MAN7 glycan

present on CD98hc. As it is a system involving three distinct proteins, the PATCHDOCK server (https://bioinfo3d.cs.tau.ac.il/PatchDock/, accessed on 10 August 2022) [45] was used to perform rigid docking, with the glycan anchored to the Asn381 from CD98hc. This site was selected as the target for interaction with ConBr, as it is the most exposed glycan and distant from the membrane. Thus, it was considered the most likely to interact with the lectin. This step was carried out exclusively to establish the ConBr–xc- complex, and the result obtained was subsequently subjected to preparation for molecular dynamics. Complexes were created with and without the presence of erastin [25].

2.7. Molecular Dynamics

Molecular dynamics simulations were prepared to evaluate the molecular behavior of the xc- system in complex with ConBr and/or erastin. Five systems were generated, which include ConBr, xc- system, xc- system + ConBr, xc- system + erastin, and xc- system + ConBr + erastin. The initial coordinates include the monomer crystallographic structure of ConBr (PDB ID: 1AZD), the structure determined by cryo-EM of the xc- system complexed with or without erastin (PDB ID: 7EPZ). Finally, the trajectories involving the ConBr complexed with the xc- system were created based on the coordinates obtained from molecular docking. Regarding the amino acid sequence of the Uniprot database, it is important to note that the PDB-derived crystallographic models do not include amino acids 1–168 for CD98hc (Uniprot ID: P08195) and 1–45 for xCT (Uniprot ID: Q9UPY5).

Inputs were processed using the web-based CHARMM-GUI server [46,47], employing the coordinates derived from the molecular docking assays. The trajectories were simulated using the pmemd.cuda module of the AMBER22 package [10], employing the ff19SB force field parameters for proteins [48], the GLYCAM_06j force field for carbohydrates [41], and Lipid17 for lipids [49].

For the trajectories, the 4 N-glycosylations of the MAN7 type and the disulfide bond between the residues Cys212 (CD98hc) and Cys160 (xCT) were included. Furthermore, the systems included calcium and manganese ions positioned within the metal binding site of ConBr, TIP3P water molecules (51,146 molecules for xc- system with/without erastin, and 54,321 molecules for xc- system with ConBr) and Na^+ (142 ions for xc- system and 171 ions for xc- system with ConBr) and Cl^- (138 ions for xc- system and 167 ions for xc- system with ConBr) counterions to neutralize the system charges. The systems involving the xc- system were embedded into a pure 1-palmitoyl-2-oleoyl-sn-glycero-3-phosphocholine (POPC, 429 molecules) membrane. Energy minimization of the systems was conducted using 10,000 steps of the steepest descent method and 5000 steps of conjugate gradient, totaling 15,000 minimization cycles, with a convergence criterion of 10 kJ/mol. After minimization, six equilibration steps followed, following a methodology commonly adopted for membrane models. The first three steps were performed at 250,000 NVT steps, while the last three were performed at 500,000 NPT steps. The temperature was maintained at 300.15 K using a Langevin thermostat, with a friction coefficient of 1 ps^{-1} [50]. Furthermore, an isotropic Monte Carlo barostat was used to control the pressure at 1 bar [51]. Covalent bonds involving hydrogen atoms were constrained by the SHAKE algorithm [52]. Long-range electrostatic interactions were calculated using the Particle Mesh Ewald (PME) method with a cutoff radius of 10 Å [53]. All simulations performed in this study lasted 400 ns, with a simulation time interval set at 2 fs.

The trajectories were analyzed concerning the root mean square deviation (RMSD) values of all atoms to verify system equilibrium and stability. To analyze the pattern of interactions between ConBr and MAN7 glycosylation from CD98hc, the intermolecular hydrogen bonds (HB) were evaluated. The analysis was performed using the AmberTools Cpptraj module on all systems [54]; Xmgrace, Pymol, and VMD have been applied for graph preparation, contacts analysis, and trajectory visualization, respectively. The last frame of the trajectories was submitted to cavity evaluation by the CaverWeb v1.2 server (https://loschmidt.chemi.muni.cz/caverweb/, accessed on 4 August 2023) [55]. Possible

tunnels and channels in the xCT protein structures were analyzed in different trajectories around the residues that interact with the substrate glutamate [24].

3. Results

3.1. Effect of ConBr on C6 Glioma Cells via Modulation of Xc- System

Initially, a dose–response curve of the antiglioma activity of ConBr (5–100 μg/mL) was carried out by assessing cell viability with MTT test, measured after 24 h of treatment. Figure 1 shows that ConBr decreases cell viability in a concentration-dependent manner.
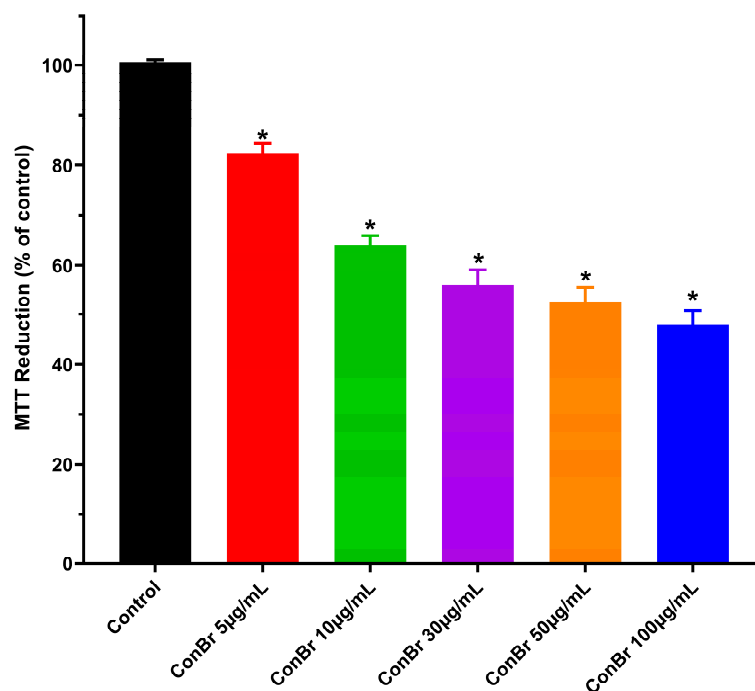

Figure 1. ConBr decreases C6 glioma cell viability. The cells were treated for 24 h with increasing concentration of ConBr and afterward incubated for 1 h with 0.5 μg/mL MTT. The data are expressed as a percentage of control. The data were analyzed with One-Way ANOVA followed by post-test Tukey. * Represents data statistically significant compared to control, *n* = 4. ConBr (*Canavalia brasiliensis* lectin).

Figure 2 shows a dose–response curve of erastin (0.5–50 μM) on C6 cell viability after 24 h treatment. The result shows that erastin promotes a drop in cell viability. Notably, the impairment of cell viability produced by erastin (10–20 μM) was of the same magnitude as that observed for ConBr (30 μg/mL; Figure 1). In the next experiments, concentrations of 30 μg/mL and 10 μM were chosen for ConBr and erastin, respectively.

Figure 3 shows a comparison of the cytotoxic activity of ConBr and erastin alone or combined. Hence, cell viability was decreased by 40% by ConBr and around 20% by erastin. However, a combination of ConBr with erastin did not improve the cytotoxicity since the cell viability impairment was similar to that observed for erastin alone. Moreover, to characterize if the ConBr effect was dependent on glycan interaction, C6 cell viability was evaluated utilizing ConBr in which the carbohydrate recognition domain (CRD) was blocked with α-methyl-mannoside (iConBr). Notable, iConBr did not cause alteration of cell viability, reinforcing that ConBr cytotoxicity depends on the lectin domain.
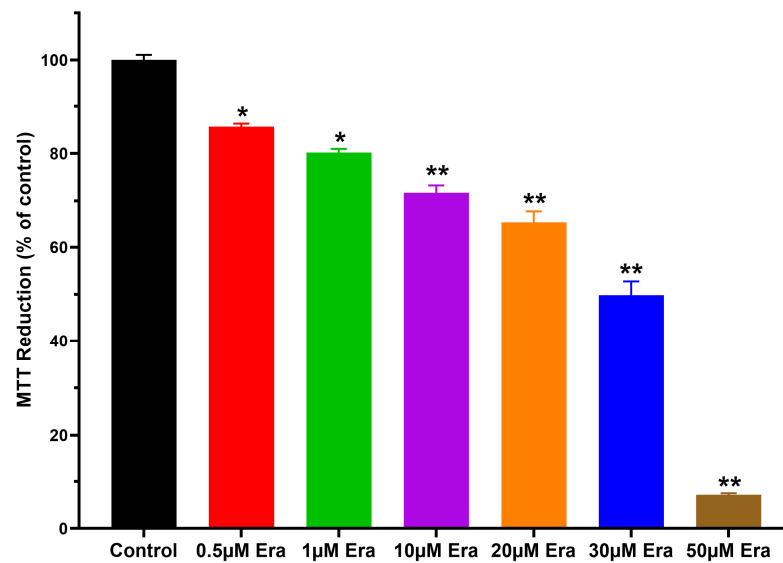
Figure 2. Erastin decreases C6 glioma cell viability in a dose-dependent manner. The cells were treated for 24 h with increasing concentration of ConBr and afterward incubated for 1 h with 0.5 μg/mL MTT. The data are expressed as a percentage of control. The data were analyzed with One-Way ANOVA followed by post-test Tukey. * Statistically significant compared to control. ** Statistically significant compared to control and previous concentration, *n* = 4. Era (erastin).
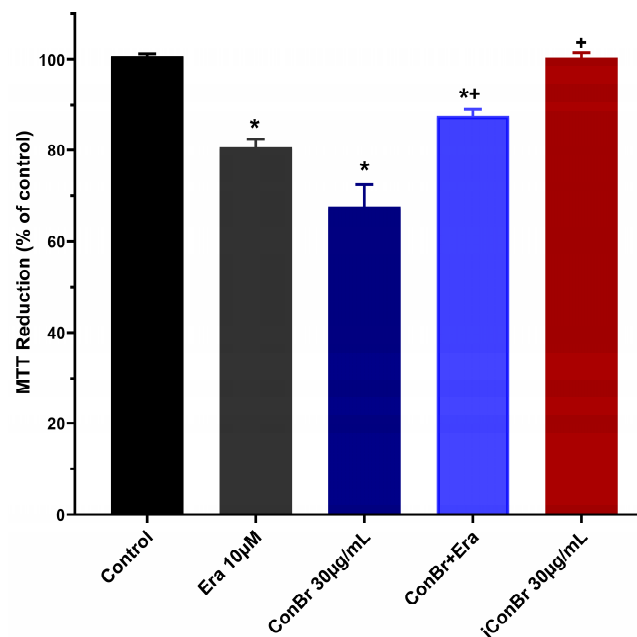

Figure 3. The co-treatment of erastin and ConBr had antagonistic effects on C6 glioma cell viability. The cells were treated for 24 h with increasing concentration of ConBr and afterward incubated for 1 h with 0.5 μg/mL MTT. The data are expressed as a percentage of control. The data were analyzed with One-Way ANOVA followed by post-test Tukey. * Statistically significant compared to control. + statistically significant compared to the ConBr group, *n* = 4. Era (erastin), ConBr (*Canavalia brasiliensis* lectin), and iConBr (ConBr blocked with α-methyl-mannoside).

We evaluated reactive species production in C6 cells in response to ConBr treatment (Figure 4) and compared it with erastin. The results show that native ConBr, but not iConBr, increases ROS production, and this effect of ConBr was greater than that observed for erastin. Notably, the combination of ConBr with erastin did not display additive cytotoxicity. Rather, it was similar to that found with erastin treatment alone.
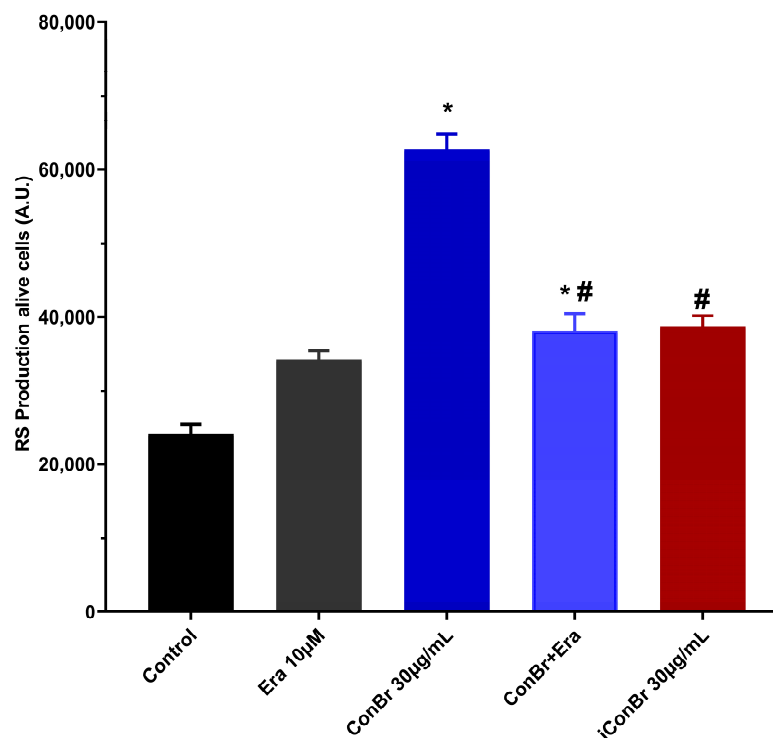
Figure 4. ConBr increases reactive species production on C6 glioma cells. The cells were treated for 24 h and afterward incubated for 30 min with 10 μM DCF-DA. The data are expressed as absolute values. The data were analyzed with One-Way ANOVA followed by post-test Tukey. * Statistically significant compared to control. # statistically significant compared to the ConBr group, *n* = 4. Era (erastin), ConBr (*Canavalia brasiliensis* lectin), and iConBr (ConBr blocked with α-methyl-mannoside).

In order to characterize a possible inhibition of the xc- system by ConBr, we measured the non-protein thiols (NPSH) in response to ConBr treatment (Figure 5). NPSH levels represent mainly the intracellular content of glutathione. The results showed that ConBr (30 μg/mL) causes a robust decrease in NPSH levels, and this effect was partially abrogated by blockage of CRD (iConBr). Erastin 10 μM, as expected, significantly decreased NPSH levels. However, combined treatment of ConBr with erastin did not improve NPSH decrease; rather, intracellular NPSH content was similar to that observed for erastin alone. Taken together, the results indicate that ConBr cytotoxicity on C6 glioma cells was dependent on lectin–glycan interaction since CRD blockage abrogated the detrimental effect of ConBr on cell viability, as well as prevented the lectin-dependent increment of RS levels and the decreasing of NPSH. These observations allow us to postulate that part of the cytotoxic mechanism of ConBr against C6 glioma cells might be due to an inhibitory interaction of ConBr with the xc- system. This possibility may be reinforced considering that (i) CD98hc is a glycoprotein with a high content of glycans; (ii) the magnitude of the ConBr effects were similar to that observed with the erastin, a classical xCT inhibitor; (iii) previous studies suggest ConA capability to inhibit the xc- system; (iv) CD98hc is recognized as a xCT modulator and monoclonal antibodies against CD98hc inhibited the xc- system. Hence, applying bioinformatics techniques, we moved to evaluate the plausibility that ConBr could modulate the xc- system via interaction with glycans present on the CD98hc regulatory subunit, using docking and molecular dynamics.
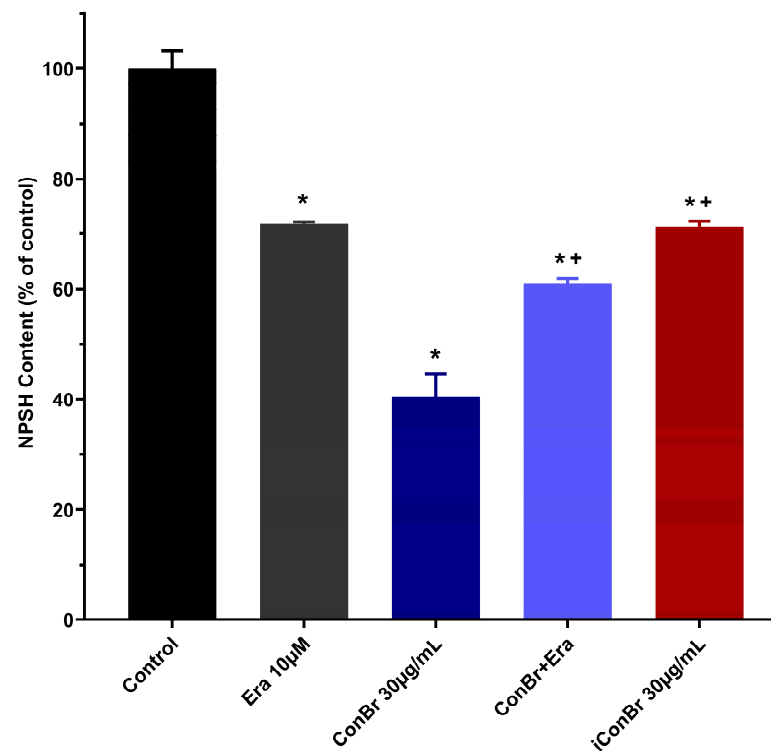
Figure 5. ConBr decreases NPSH content. The cells were treated for 24 h with the drugs, and afterward, the cells were rinsed. The non-protein total thiol quantification (NPSH) was performed by Ellmann's reaction. The data are expressed as a percentage of control. The data were analyzed with One-Way ANOVA followed by post-test Tukey. * Statistically significant compared to control. + statistically significant compared to the ConBr group, n = 4. Era (erastin), ConBr (*Canavalia brasiliensis* lectin), and iConBr (ConBr blocked with α-methyl-mannoside).

3.2. Molecular Docking

The score values obtained (in arbitrary units) by molecular docking between ConBr and CD98hc N-glycans are presented in Table 1, mainly GlcNAc2Man7 (MAN7), with a score of −58.42. ConBr demonstrated favorable affinity with high mannose N-glycans and lower affinity with complex N-glycans with one terminal fucosyl. No favorable interaction results were observed with complex N-glycans double terminal fucosylation or with fucosylation simultaneously at the terminal and core. Subsequently, MAN7 was inserted into the four glycosylation sites of CD98hc, and ConBr was fixed in interaction with one of these sites using the PatchDock v. 1.3 software using rigid docking [45,56]. The interaction involved residues present in the carbohydrate recognition domain (CRD) of the lectin, forming a network of hydrogen bonds that included the amino acids Tyr12, Asn14, Thr15, Asp16, Leu99, Tyr100, Ser168, Asp208, and Arg228.

Table 1. Molecular docking scores of the interactions between ConBr and N-glycans present in CD98hc (according to Powlesland et al. (2009) [40]. In glycan structure diagrams is N-acetyl-D-glucosamine (GlcNAc), mannose (Man), galactose (Gal), and fucose (Fuc).

Glycan	Structure	Docking Score
GlcNAc$_2$Man$_7$		−58.42

Table 1. *Cont.*

Glycan	Structure	Docking Score
GlcNAc$_2$Man$_8$		−49.30
GlcNAc$_2$Man$_9$		−51.31
GlcNAc$_2$Man$_3$GlcNAc$_2$Gal$_2$Fuc		−43.19
GlcNAc$_2$Man$_3$GlcNAc$_3$Gal$_3$Fuc		−48.11
FucGlcNAc$_2$Man$_3$GlcNAc$_2$Gal$_2$Fuc$_2$		-
FucGlcNAc$_2$Man$_3$GlcNAc$_2$Gal$_2$Fuc		-
FucGlcNAc$_2$Man$_3$GlcNAc$_3$Gal$_3$Fuc		-

3.3. Molecular Dynamics

Regarding the molecular dynamics trajectories, a total of five trajectories were performed to evaluate the behavior of ConBr, CD98hc, and xCT in different conditions. All trajectories were run for 400 ns (20,000 frames) under a pressure of 1 bar, temperature of 300.15 K, pH 7.0, and in the presence of 0.15 M NaCl. All trajectories occurred as expected, without artifacts. In all simulations involving the xc- system, the complex remained surrounded by the lipid bilayer through the xCT protein. In the simulation involving the xc-system and erastin, the drug remained interacting with the complex until the end of the trajectory. The ConBr + xc- system + erastin system can be observed in Figure 6A, where the interaction of ConBr with MAN7 via CRD is evident (Figure 6B), while erastin is complexed between the xCT transmembrane helices (Figure 6C). In the simulation involving the ConBr + xc- system, ConBr remained interacting with CD98hc until the end of the trajectory through interaction with MAN7 (Figure 7A). However, it was not possible to obtain a stable trajectory with ConBr in the xc- system in the simulation involving ConBr + xc- system + erastin, as ConBr always disconnected from the complex at some point in the trajectory. In the presented trajectory, ConBr releases between 100–120 ns (Figure 7B).
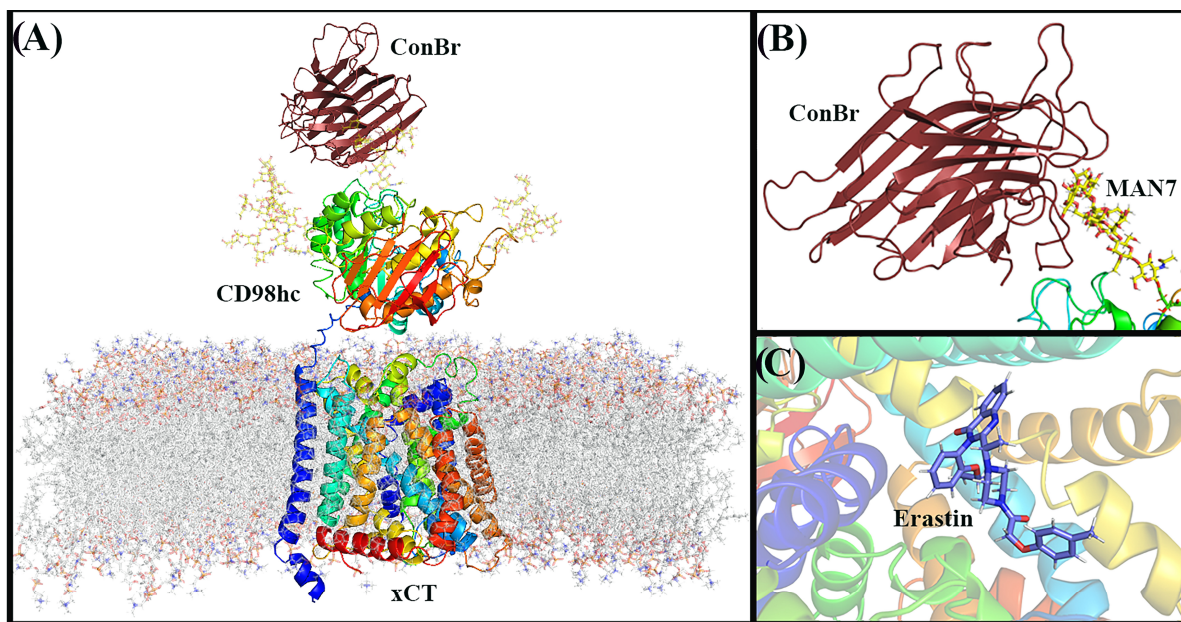
Figure 6. Complex formed by ConBr with the xc- and erastin system: (**A**) System composed of the xc-system formed by the extracellular protein CD98hc and the transmembrane protein xCT inserted into the lipid bilayer formed by POPC. ConBr interacts with the CD98hc protein via N-glycosylation; (**B**) Interaction of ConBr with MAN7 glycan anchored on CD98hc; (**C**) Erastin molecule complexed between the xCT transmembrane helices. The proteins are represented in cartoon format, with the xc- system in rainbow and ConBr in red. The four N-glycans molecules of MAN7 (carbons in yellow), erastin (carbons in purple), and POPC molecules (carbons in gray) are represented in stick representation.
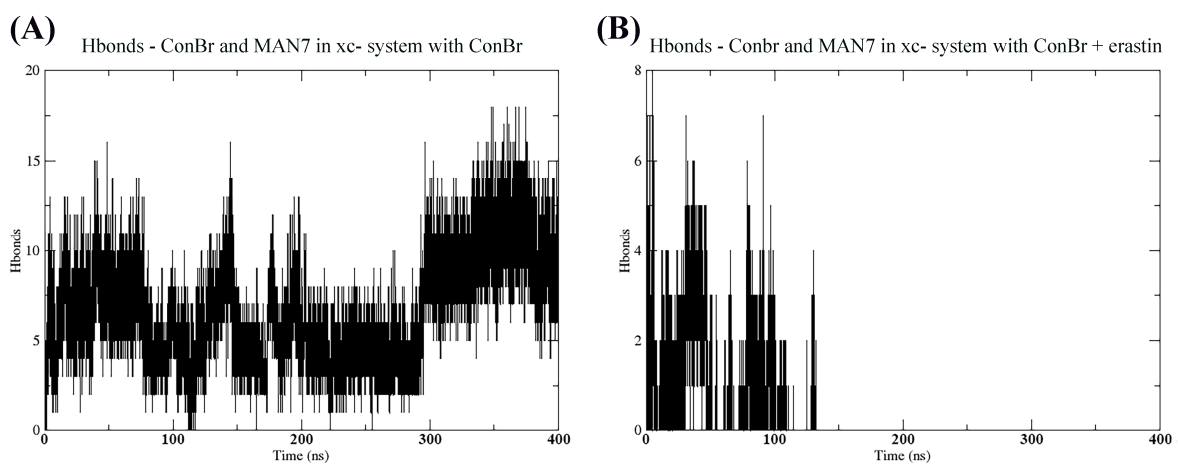

Figure 7. The number of hydrogen interactions between ConBr and MAN7 N-glycan present in CD98hc. (**A**) ConBr + xc- system trajectory; (**B**) ConBr + xc- system + erastin trajectory.

Through the RMSD graphs, we can observe that ConBr reached equilibrium in all trajectories, presenting higher deviations when in complex with the xc- system than in the lectin trajectory (Figure 8A). This demonstrates that the interaction with MAN7 and CD98hc has an impact on the lectin structure. It is important to highlight that in the simulation containing ConBr + xc system- + erastin, ConBr detached from the complex around 100–120 ns and then showed non-specific interactions on the surface of the system and with the aqueous medium. CD98hc reached equilibrium easily in three systems, and it was only in the presence of erastin that the protein was more unstable, although it showed constant behavior throughout the trajectory (Figure 8B). ConBr resulted in slightly higher

deviation values for CD98hc but was able to stabilize the protein throughout the simulation. Given that the interaction of erastin occurs with the xCT protein, drug complexation stabilizes xCT, but causes instability in CD98hc, probably by affecting the intermolecular interactions that regulate the complex. In the ConBr + xc- system + erastin trajectory, a deviation of around 100–120 ns was observed at the moment when ConBr disconnected from the complex. However, CD98hc continues to behave in a similar way to the native protein for the remainder of the simulation, even with erastin in a complex with xCT (Figure 8C). In the ConBr + xc- system + erastin trajectory, the ConBr interaction time was able to stabilize CD98hc without impacts on xCT (Figure 8B), as the transporter showed similar behavior to the system in the presence of erastin alone (Figure 8C). In the case of xCT, the protein reached equilibrium quickly in all systems. However, clearly larger deviations were observed when ConBr was present in the trajectory without erastin. Therefore, it can be noted that the interaction of ConBr with CD98hc has a greater influence on the structure of xCT than the interaction with erastin. When evaluating the xc- system as a whole, it was observed that in the trajectory in the presence of ConBr and erastin, there is a low impact on the structure of the system (Figure 8D). On the other hand, isolated erastin presents high deviations, mainly due to the unstable behavior of CD98hc in this trajectory. Finally, ConBr alone has an impact on CD98hc and xCT, suggesting that ConBr modifies the way CD98hc regulates xCT.
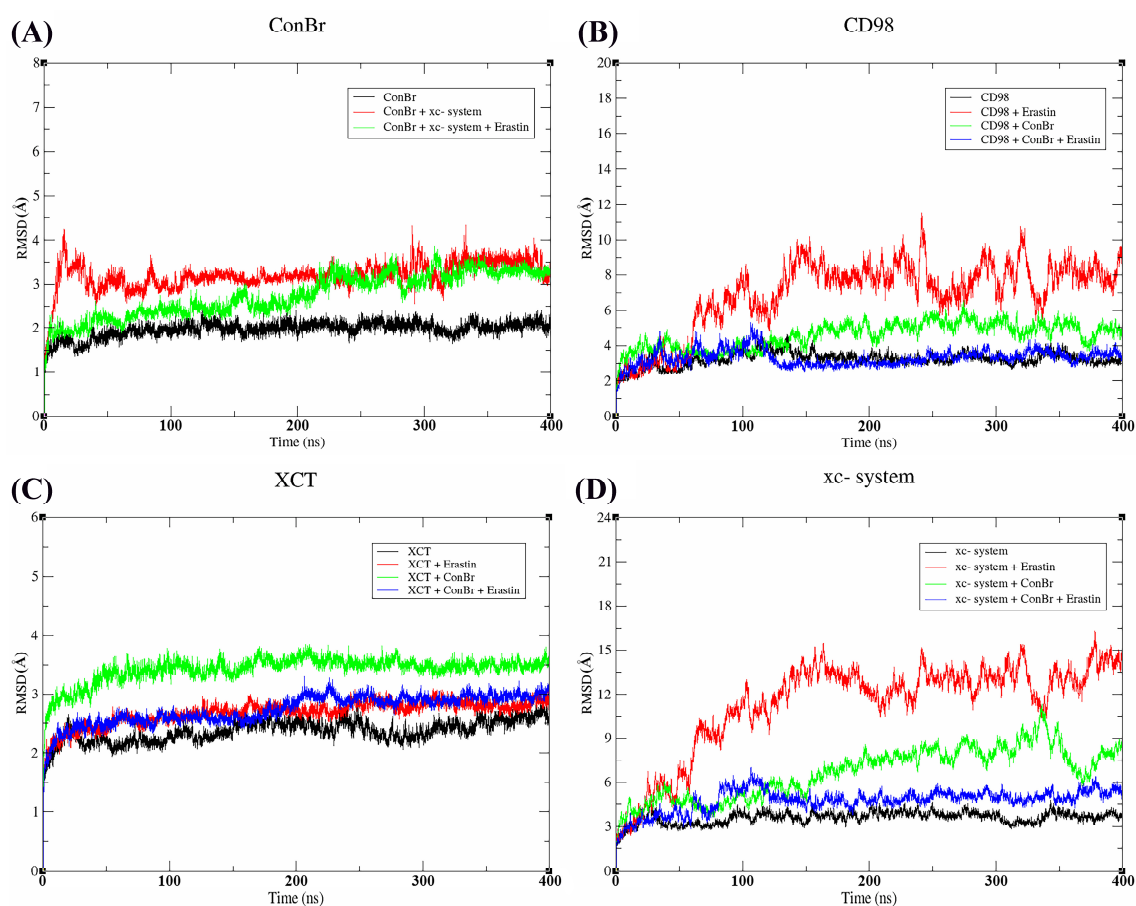

Figure 8. Root mean square deviation (RMSD) plots of molecular dynamics trajectories. (**A**) ConBr; (**B**) CD98hc; (**C**) xCT and (**D**) xc- system.

Differences in conformations can be observed through snapshots of the trajectories. Figure 9A–C correspond to times 0, 200, and 400 ns of the xc- system, while Figure 9D–F depict the xc- system complexed with erastin. Furthermore, Figure 10A–C represent the xc- system complexed with ConBr, and finally, Figure 10D–F show the xc- system complexed

with ConBr and erastin. It is important to highlight that, in the latter case, it is possible to observe the ConBr disconnecting from the receiver during the trajectory. In trajectories in the presence of erastin, interactions at the interface between the two proteins are smaller. In Figure 9D–F, the distance of the interfaces between the two proteins increases, and a decrease in the number of contacts was observed (Figure 11A,B). In the trajectories with the presence of ConBr, there was more contact in the interface region (Figures 10A–C and 11C). However, in the trajectory where there is ConBr and erastin, ConBr interacts with the receptor until about 100 ns, but the effect of intensifying interactions in the interface region remains. This greater contact may be associated with an intensified regulation of CD98hc on xCT, causing conformational changes in the transmembrane helices of xCT and altering the transport activity.
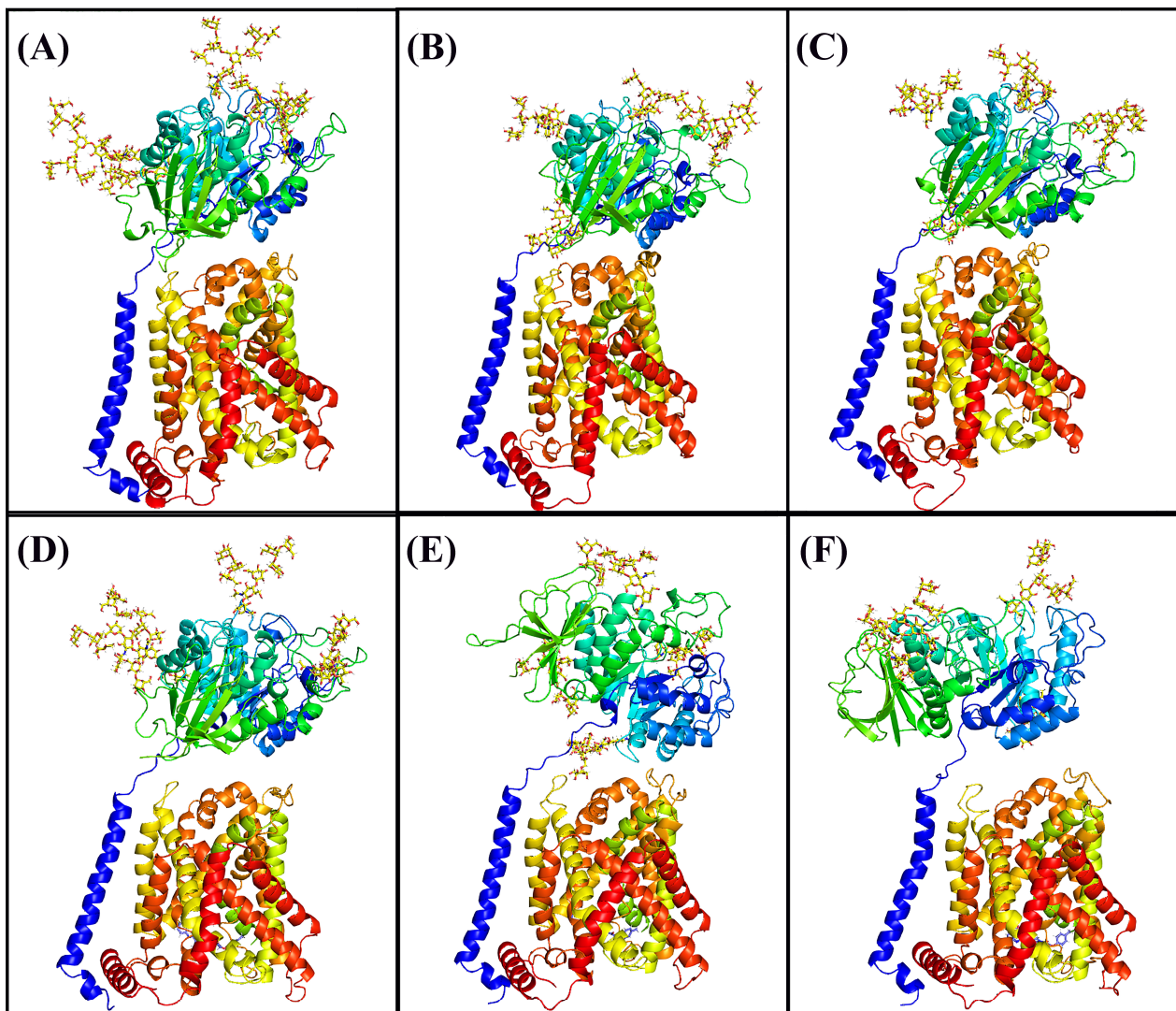

Figure 9. Snapshots from molecular dynamics trajectories. (**A**) 0 ns interval of the xc- system trajectory; (**B**) 200 ns interval of the xc- system trajectory; (**C**) 400 ns interval of the xc- system trajectory; (**D**) 0 ns interval of xc- system + erastin trajectory; (**E**) 200 ns interval of the trajectory of xc- system + erastin; (**F**) 400 ns interval of the trajectory of xc- system + erastin. Proteins are in cartoon representation colored in a rainbow, while erastin is in stick representation with carbon colored in purple.
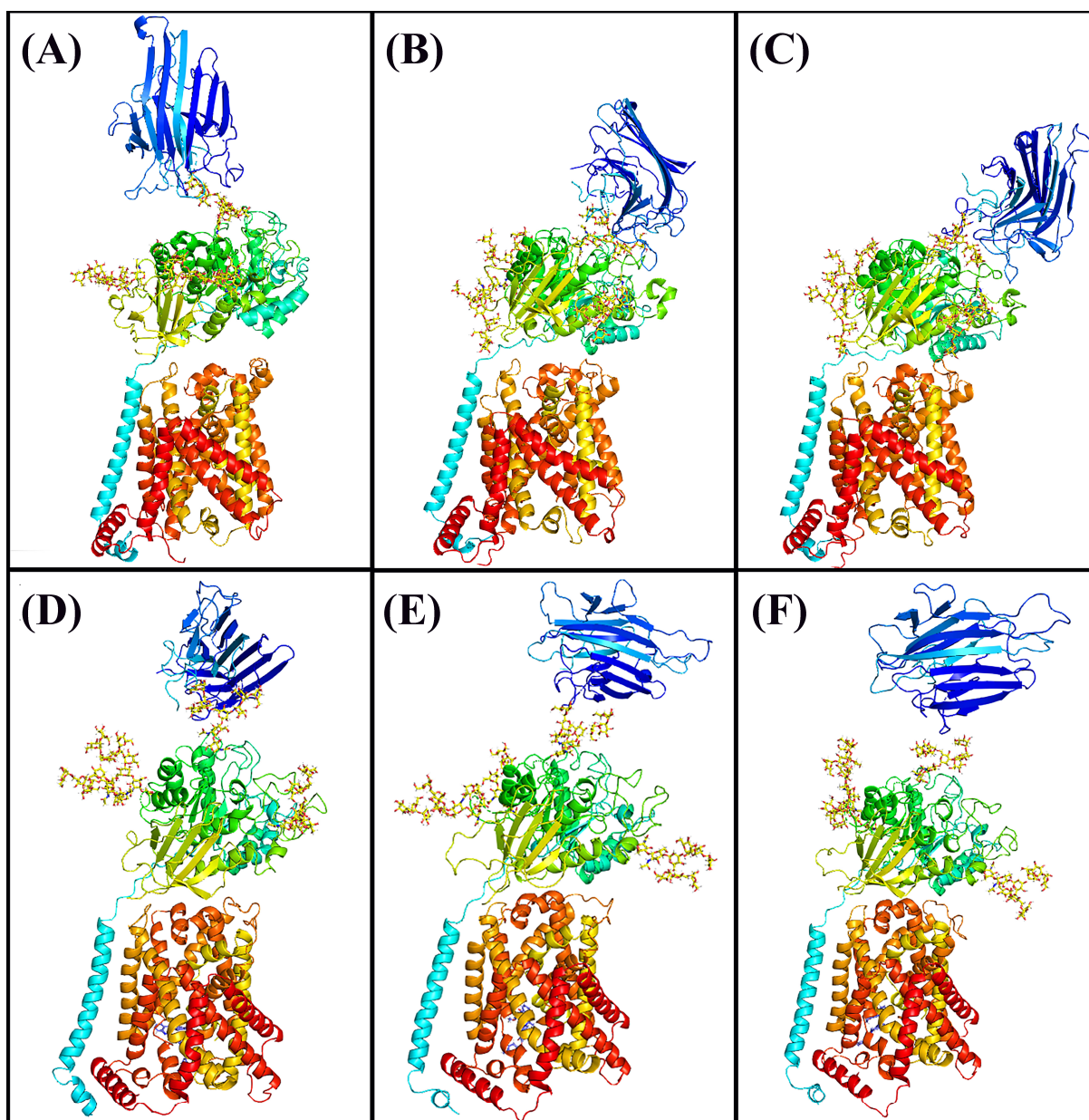
Figure 10. Snapshots from molecular dynamics trajectories. (**A**) 0 ns interval of the ConBr + xc-system trajectory; (**B**) 200 ns interval of the ConBr + xc- system trajectory; (**C**) 400 ns interval of the ConBr + xc- system trajectory; (**D**) 0 ns interval of ConBr + xc- system + erastin trajectory; (**E**) 200 ns interval of the trajectory of ConBr + xc- system + erastin; (**F**) 400 ns interval of the trajectory of ConBr + xc- system + erastin. ConBr (in blue) and xc- system (in rainbow) are in cartoon representation, while erastin is in stick representation with carbon colored in purple.

When evaluating the final frames by the CaverWeb server and using the input cavity and glutamate interaction residues (Arg135, Tyr244, Phe250, Tyr251, Gly334, and Arg396) as a reference, a length change in the transporter tunnels was observed (Figure 12). The native xCT has a length of 156.3 Å, while in complex with erastin, it has 112.6 Å; in complex with ConBr, it has a length of 62.8 Å, and in the presence of ConBr and erastin, it has a length of 136 Å.
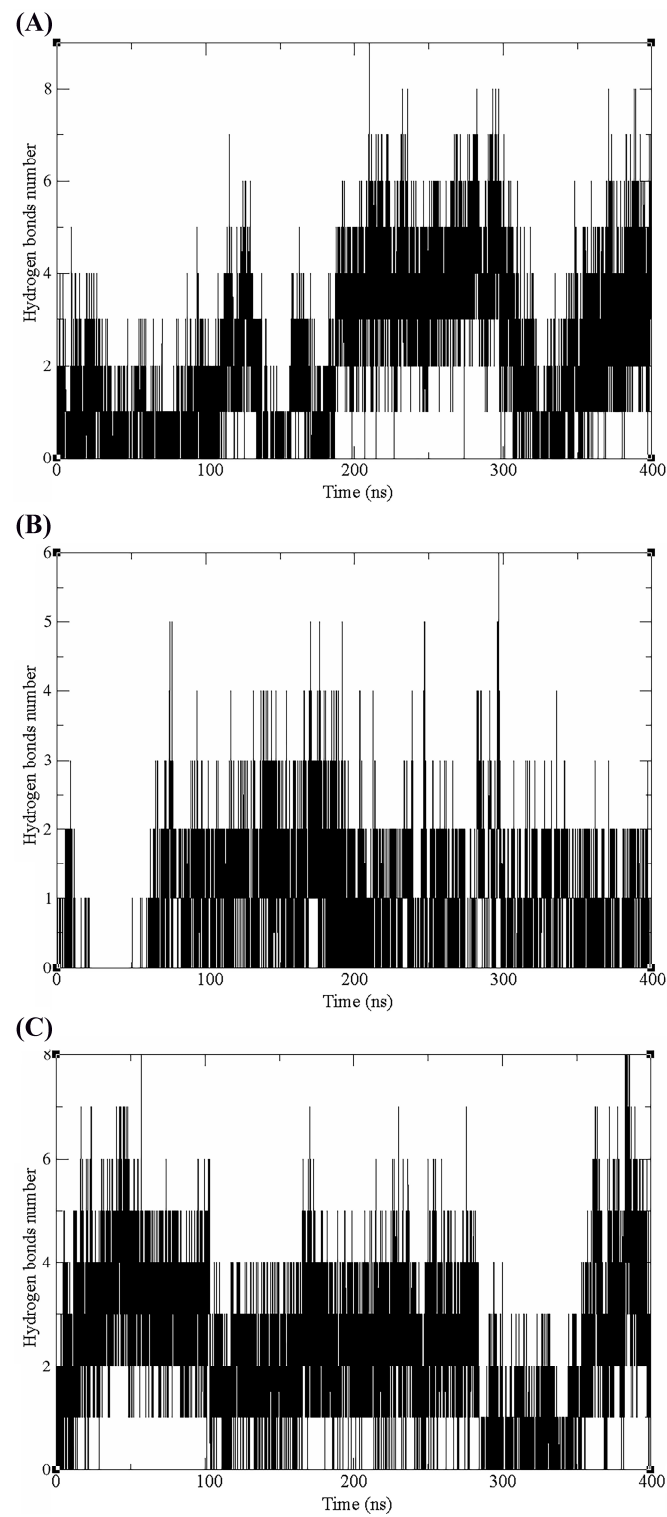
Figure 11. The number of hydrogen bonds between the CD98hc and xCT interface in the trajectories: (**A**) xc- system; (**B**) xc- system + erastin and (**C**) xc- system + ConBr.
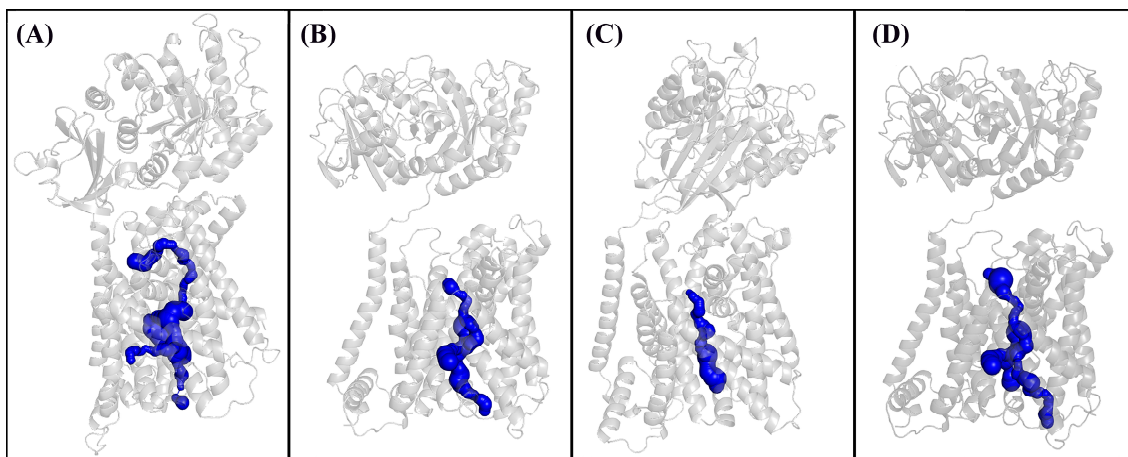
Figure 12. Evaluate the tunnel length of the glutamate entry cavity in xCT through the CaverWeb v1.2 server using the last frame of the trajectories: (**A**) xc- system; (**B**) xc- system + erastin; (**C**) xc- system + ConBr; (**D**) xc- system + ConBr + erastin. xc- system is represented in gray in cartoon format, and the tunnels are highlighted in blue.

4. Discussion

Lectins, one of the main groups of carbohydrate-binding proteins, have been shown to be interesting anticancer agents, particularly in glioma. ConBr, a ConA-like lectin, is one of the lectins demonstrating anticancer effects against glioma cells [13]. ConBr significantly reduced the viability of C6 glioma cells at doses as low as 50 μg/mL, and the data revealed the antiglioma effect elicited by the lectin is mediated through controlled cell death mechanisms dependent on the binding between ConBr and glycoconjugates on the cell surface. The primary mechanism behind the observed effects is related to the modulation of the MAPKs and Akt signaling pathways, which leads to the activation of autophagic mechanisms in a caspase-8-dependent manner [13]. This capacity is not unique to ConBr, with several other ConA-like lectins displaying similar cytotoxicity profiles through similar routes, such as lectins from *Dioclea lasiophylla* and *C. grandiflora* seeds [14,15]. Previous data have revealed that ConA modulates the activity and expression of matrix metalloproteinases (MMPs) in glioma cells, which includes influencing MT1-MMP. This modulation contributes to various cellular processes crucial in the context of glioma pathologies—such as cell migration, invasion, and survival—and it appears to be closely linked to the antiglioma effect demonstrated by the lectin—where it modulates both the expression and activity of the enzyme, contributing to changes in cell migration, invasion, and survival [57,58]. Another mechanism of ConA-like lectins has been suggested by [14]. In a study involving *C. grandiflora* (ConGF) lectin, the authors suggested a possible interaction between ConGF and glycan structures of MMP1, a prominent protein found in gliomas. This binding would lead to the inhibition of MMP1, resulting in a downregulation of PAR1 and downstream pathways, including ERK1/2 and AKT/mTOR.

Erastin, an inhibitor of the xCT subunit (SLC7A11) of the xc-antiporter, is well known to promote a cytotoxic effect on tumor cells, mainly due to the reduction of cystine uptake and consequent glutathione synthesis. This event causes cell redox imbalance, ending with lipid peroxidation and cell death by a mechanism known as ferroptosis [25,28,29,38].

It has been demonstrated that CD98hc (SLC3A2), the regulatory heavy chain of the xc-system, is a protein highly glycosylated, which plays an important role in the regulation of xc-antiporter via interaction with the cystine/glutamate transporter subunit xCT [24,32–34]. As stated previously, via the xc- system, cystine is incorporated into the intracellular environment, followed by a reduction to cysteine that will be used to synthesize glutathione (GSH), a powerful intracellular antioxidant [26,27]. This system is positively regulated in gliomas and confers a tumor growth advantage [27]. Importantly, in myeloma multiple, the

glycans that decorate the CD98hc surface were demonstrated to be targets for monoclonal antibodies that promoted selective tumor cell death [35].

Molecular docking results corroborate the documented findings on the specificity of ConBr for carbohydrates, a lectin that demonstrated an affinity for high-mannose N-glycans [9]. This pattern has already been widely observed and described in the interaction between ConA-type lectins and high-mannose N-glycans [59]. The composition of the glycans present on CD98hc is well reported, showing that CD98hc contains complex-type N-glycans composed of 5 to 11 hexose residues, 4 to 10 N-acetylhexosamine residues, and 1 to 6 fucose residues, structurally represented with structures bi- and tri-antennary with terminal fucosylation and sialylation and with high mannose content [40]. ConBr, a ConA-like lectin, has a preference for diglycoside and dimanoside residues with a preference for dimanosides with $\alpha 1,2$ and $\alpha 1,6$ linkages and strong binding to the trimmannoside nucleus of the N-glycans [60]. It opens up several new opportunities for biomedical applications not only for ConBr but also for a variety of glucose/mannose-specific lectins. CD98hc could covalently associate with other proteins, called light subunits, as is the case with xCT itself and large neutral amino acid transporters (LATs). These complexes are closely linked to various functions, such as cell adhesion, energy metabolism, and hormone transport, and represent potential targets for therapies against some types of brain cancer, such as gliomas [26,61–63].

From the molecular dynamics evaluation, it was possible to observe and analyze the behavior of the xc- system in the presence of ConBr and/or erastin. Studies show that erastin is a molecule classically used to inhibit the system and induce ferroptosis [64]. Despite being a specific and potent inhibitor, erastin causes fewer changes in cavity length than ConBr. This is due to the fact that erastin binds to a site other than the glutamate-binding pocket on the xCT. The chlorophenoxy group in the erastin molecule functionally interacts with the Phe254 in the TM6b domain of xCT, thereby mediating the inhibitory effects [25]. Thus, this molecule prevents the system from functioning by sterically blocking the entry of glutamate into the cavity without necessarily changing the structure of the tunnel. On the other hand, ConBr is probably capable of altering the tunnel and affecting glutamate/cystine transport, promoting ferroptosis. CD98hc interacts with xCT at the interface between the two proteins and in the transmembrane region, mainly through polar and hydrophobic interactions. CD98hc has a transmembrane helix (TM) and a short helix called H1' that interacts with xCT through the H4 helix, which traps xCT on the intracellular side [25]. In this context, ConBr is capable of interacting with CD98hc, which intensifies intermolecular contacts with xCT, causing conformational changes in the transmembrane region and closing the glutamate/cystine transport channel. The presence of erastin apparently reduces the impact of these effects promoted by ConBr or vice versa. The results obtained from the evaluation of the tunnels and the inhibition potential of xCT correlate well with the findings of our in vitro tests with ConBr and erastin concerning the changes of C6 glioma cell viability, as well as reactive species production and decrease of NPSH.

Our bioinformatic study indicates that the interaction of lectin with CD98hc glycans can inhibit the xc- system and thus explain the increment of RS and reduced antioxidant defense (glutathione) observed. In this direction, a previous study showed ConA modulating thiol-disulfide balance in C6 glioma cells and triggering oxidative damage [65]. Moreover, ConA was also known as an inducer of ferroptosis, especially in the context of liver cells [66,67]. In this model, through an unknown mechanism, ConA caused downregulation of the xCT subunit, reducing GSH synthesis and consequently triggering oxidative stress, lipid peroxidation, and cell death by ferroptosis. Considering the similarity between ConBr and ConA, it is not a stretch to assume that the former is able to activate the same pathways, thus being able to induce ferroptosis. However, these points deserve to be deeply investigated in the future.

Therefore, our study contributes to the understanding that the mechanism of oxidative stress and possibly ferroptosis, triggered by ConA-like lectins, may primarily involve

interaction with the CD98hc glycans. This demonstration is a basic study that suggests a potential application of this knowledge as a strategy to selectively ascertain tumor cells and, by disturbing redox pathways, induce glioma cell death. Modification of glycans on glioma cell surface has been described [5,6]. Nevertheless, there is no description at the moment of specific alteration of CD98hc glycans in gliomas. Notably, one study showed selective myeloma multiple tumor cell death by monoclonal antibodies against CD98hc glycans without disturbing normal cells [35]. Therefore, modification of glycan structure on CD98hc glycoprotein or increment of its expression on the tumor cell surface could be a direct target for lectins or, alternatively, for nanostructures containing lectin and antitumor agents. This strategy could improve selective cell attack and cell death.

5. Conclusions

The glucose/mannose-specific lectin from *Canavalia brasiliensis* seeds, called ConBr, was able to induce cell death in C6 glioma cells, increasing reactive oxygen species and decreasing thiol groups. The effect promoted by the lectin was dependent on the activity of the carbohydrate recognition domain and was more intense than that observed for erastin. However, when tested together, an antagonistic effect was observed. This finding was supported by bioinformatics data, which demonstrated that ConBr could regulate the xCT transporter through interaction with glycans present on CD98hc. This was the first study in which the regulation of the xc- system by lectins was structurally demonstrated. Furthermore, they suggest the potential of lectins to promote ferroptosis through regulation of the xc- system in glioma cells.

Author Contributions: Conceptualization, V.R.P.-J., R.B.L. and B.S.C.; methodology, V.R.P.-J., R.L.S., C.H.D.S.-F., A.P.F., N.S., M.V.O. and V.J.S.O.; validation, V.R.P.-J., R.L.S., C.H.D.S.-F., A.P.F., N.S., M.V.O., V.J.S.O., K.S.N., R.B.L. and B.S.C.; formal analysis, V.R.P.-J., R.L.S., C.H.D.S.-F., A.P.F., N.S., M.V.O., V.J.S.O., K.S.N., R.B.L. and B.S.C.; resources, K.S.N., R.B.L. and B.S.C.; investigation, V.R.P.-J., R.L.S., C.H.D.S.-F., A.P.F., N.S., M.V.O., V.J.S.O., K.S.N., R.B.L. and B.S.C.; writing—original draft preparation, V.R.P.-J., M.V.O., V.J.S.O. and R.B.L.; writing—review and editing, V.R.P.-J., M.V.O., V.J.S.O., K.S.N., R.B.L. and B.S.C.; supervision, K.S.N., R.B.L. and B.S.C.; project administration, K.S.N., R.B.L. and B.S.C.; funding acquisition, K.S.N., R.B.L. and B.S.C. All authors have read and agreed to the published version of the manuscript.

Institutional Review Board Statement: This study was performed in compliance with the Helsinki Declaration on ethical principles for handling human tissue specimens, with all Brazilian national regulations and requirements. Rat C6 glioma cells (ATCC-CCL-107) lineages were provided by the Cell Bank of Rio de Janeiro (RJ, Brazil).

Data Availability Statement: The data supporting the findings of this study are available within the article. Data available on request from the authors.

Conflicts of Interest: The authors have declared that no conflicts of interest are associated with this publication.

References

1. Weller, M.; Wick, W.; Aldape, K.; Brada, M.; Berger, M.; Pfister, S.M.; Nishikawa, R.; Rosenthal, M.; Wen, P.Y.; Stupp, R.; et al. Glioma. *Nat. Rev. Dis. Prim.* **2015**, *1*, 15017. [CrossRef]
2. Horbinski, C.; Berger, T.; Packer, R.J.; Wen, P.Y. Clinical Implications of the 2021 Edition of the WHO Classification of Central Nervous System Tumours. *Nat. Rev. Neurol.* **2022**, *18*, 515–529. [CrossRef]

3. Reifenberger, G.; Wirsching, H.-G.; Knobbe-Thomsen, C.B.; Weller, M. Advances in the Molecular Genetics of Gliomas—Implications for Classification and Therapy. *Nat. Rev. Clin. Oncol.* **2017**, *14*, 434–452. [CrossRef]

4. Yool, A.J.; Ramesh, S. Molecular Targets for Combined Therapeutic Strategies to Limit Glioblastoma Cell Migration and Invasion. *Front. Pharmacol.* **2020**, *11*, 358. [CrossRef] [PubMed]

5. Furukawa, J.-I.; Tsuda, M.; Okada, K.; Kimura, T.; Piao, J.; Tanaka, S.; Shinohara, Y. Comprehensive Glycomics of a Multistep Human Brain Tumor Model Reveals Specific Glycosylation Patterns Related to Malignancy. *PLoS ONE* **2015**, *10*, e0128300. [CrossRef]

6. Yue, J.; Huang, R.; Lan, Z.; Xiao, B.; Luo, Z. Abnormal Glycosylation in Glioma: Related Changes in Biology, Biomarkers and Targeted Therapy. *Biomark. Res.* **2023**, *11*, 54. [CrossRef] [PubMed]

7. van Solinge, T.S.; Nieland, L.; Chiocca, E.A.; Broekman, M.L.D. Advances in Local Therapy for Glioblastoma—Taking the Fight to the Tumour. *Nat. Rev. Neurol.* **2022**, *18*, 221–236. [CrossRef] [PubMed]

8. Bhutia, S.K.; Panda, P.K.; Sinha, N.; Praharaj, P.P.; Bhol, C.S.; Panigrahi, D.P.; Mahapatra, K.K.; Saha, S.; Patra, S.; Mishra, S.R.; et al. Plant Lectins in Cancer Therapeutics: Targeting Apoptosis and Autophagy-Dependent Cell Death. *Pharmacol. Res.* **2019**, *144*, 8–18. [CrossRef] [PubMed]

9. Cavada, B.S.; Osterne, V.J.S.; Pinto-Junior, V.R.; Nascimento, K.S. ConBr, the Lectin from Canavalia Brasiliensis Mart. Seeds: Forty Years of Research. *Curr. Protein Pept. Sci.* **2019**, *20*, 600–613. [CrossRef] [PubMed]

10. Gautam, A.K.; Sharma, D.; Sharma, J.; Saini, K.C. Legume Lectins: Potential Use as a Diagnostics and Therapeutics against the Cancer. *Int. J. Biol. Macromol.* **2020**, *142*, 474–483. [CrossRef]

11. Mazalovska, M.; Kouokam, J.C. Plant-Derived Lectins as Potential Cancer Therapeutics and Diagnostic Tools. *BioMed Res. Int.* **2020**, *2020*, 1631394. [CrossRef] [PubMed]

12. Pace, A.; Scirocchi, F.; Napoletano, C.; Zizzari, I.G.; D'Angelo, L.; Santoro, A.; Nuti, M.; Rahimi, H.; Rughetti, A. Glycan-Lectin Interactions as Novel Immunosuppression Drivers in Glioblastoma. *Int. J. Mol. Sci.* **2022**, *23*, 6312. [CrossRef] [PubMed]

13. Wolin, I.A.V.; Heinrich, I.A.; Nascimento, A.P.M.; Welter, P.G.; Sosa, L.D.V.; De Paul, A.L.; Zanotto-Filho, A.; Nedel, C.B.; Lima, L.D.; Osterne, V.J.S.; et al. ConBr Lectin Modulates MAPKs and Akt Pathways and Triggers Autophagic Glioma Cell Death by a Mechanism Dependent upon Caspase-8 Activation. *Biochimie* **2021**, *180*, 186–204. [CrossRef] [PubMed]

14. Leal, R.B.; Mann, J.; Pinto-Junior, V.R.; Oliveira, M.V.; Osterne, V.J.S.; Wolin, I.A.V.; Nascimento, A.P.M.; Welter, P.G.; Ferreira, V.M.S.; Silva, A.A.; et al. Structural Prediction and Characterization of Canavalia Grandiflora (ConGF) Lectin Complexed with MMP1: Unveiling the Antiglioma Potential of Legume Lectins. *Molecules* **2022**, *27*, 7089. [CrossRef] [PubMed]

15. Leal, R.B.; Pinto-Junior, V.R.; Osterne, V.J.S.; Wolin, I.A.V.; Nascimento, A.P.M.; Neco, A.H.B.; Araripe, D.A.; Welter, P.G.; Neto, C.C.; Correia, J.L.A.; et al. Crystal Structure of DlyL, a Mannose-Specific Lectin from Dioclea Lasiophylla Mart. Ex Benth Seeds That Display Cytotoxic Effects against C6 Glioma Cells. *Int. J. Biol. Macromol.* **2018**, *114*, 64–76. [CrossRef] [PubMed]

16. Nascimento, A.P.M.; Knaut, J.L.; Rieger, D.K.; Wolin, I.A.V.; Heinrich, I.A.; Mann, J.; Juarez, A.V.; Sosa, L.D.V.; De Paul, A.L.; Moreira, C.G.; et al. Anti-Glioma Properties of DVL, a Lectin Purified from Dioclea Violacea. *Int. J. Biol. Macromol.* **2018**, *120*, 566–577. [CrossRef] [PubMed]

17. Nascimento, K.S.; Andrade, M.L.L.; Silva, I.B.; Domingues, D.L.; Chicas, L.S.; Silva, M.T.L.; Bringel, P.H.S.F.; Marques, G.F.O.; Martins, M.G.Q.; Lóssio, C.F.; et al. Heterologous Production of α-Chain of *Dioclea sclerocarpa* Lectin: Enhancing the Biological Effects of a Wild-Type Lectin. *Int. J. Biol. Macromol.* **2020**, *156*, 1–9. [CrossRef] [PubMed]

18. Krishna, S.; Choudhury, A.; Keough, M.B.; Seo, K.; Ni, L.; Kakaizada, S.; Lee, A.; Aabedi, A.; Popova, G.; Lipkin, B.; et al. Glioblastoma Remodelling of Human Neural Circuits Decreases Survival. *Nature* **2023**, *617*, 599–607. [CrossRef] [PubMed]

19. Pereira, M.S.L.; Klamt, F.; Thomé, C.C.; Worm, P.V.; de Oliveira, D.L. Metabotropic Glutamate Receptors as a New Therapeutic Target for Malignant Gliomas. *Oncotarget* **2017**, *8*, 22279–22298. [CrossRef]

20. Venkataramani, V.; Tanev, D.I.; Strahle, C.; Studier-Fischer, A.; Fankhauser, L.; Kessler, T.; Körber, C.; Kardorff, M.; Ratliff, M.; Xie, R.; et al. Glutamatergic Synaptic Input to Glioma Cells Drives Brain Tumour Progression. *Nature* **2019**, *573*, 532–538. [CrossRef]

21. Venkatesh, H.S.; Morishita, W.; Geraghty, A.C.; Silverbush, D.; Gillespie, S.M.; Arzt, M.; Tam, L.T.; Espenel, C.; Ponnuswami, A.; Ni, L.; et al. Electrical and Synaptic Integration of Glioma into Neural Circuits. *Nature* **2019**, *573*, 539–545. [CrossRef] [PubMed]

22. Pratt, J.; Annabi, B. Induction of Autophagy Biomarker BNIP3 Requires a JAK2/STAT3 and MT1-MMP Signaling Interplay in Concanavalin-A-Activated U87 Glioblastoma Cells. *Cell. Signal.* **2014**, *26*, 917–924. [CrossRef]

23. Pratt, J.; Iddir, M.; Bourgault, S.; Annabi, B. Evidence of MTCBP-1 Interaction with the Cytoplasmic Domain of MT1-MMP: Implications in the Autophagy Cell Index of High-Grade Glioblastoma. *Mol. Carcinog.* **2016**, *55*, 148–160. [CrossRef] [PubMed]

24. Parker, J.L.; Deme, J.C.; Kolokouris, D.; Kuteyi, G.; Biggin, P.C.; Lea, S.M.; Newstead, S. Molecular Basis for Redox Control by the Human Cystine/glutamate Antiporter System Xc. *Nat. Commun.* **2021**, *12*, 7147. [CrossRef] [PubMed]

25. Yan, R.; Xie, E.; Li, Y.; Li, J.; Zhang, Y.; Chi, X.; Hu, X.; Xu, L.; Hou, T.; Stockwell, B.R.; et al. The Structure of Erastin-Bound xCT-4F2hc Complex Reveals Molecular Mechanisms Underlying Erastin-Induced Ferroptosis. *Cell Res.* **2022**, *32*, 687–690. [CrossRef] [PubMed]

26. Liu, J.; Xia, X.; Huang, P. xCT: A Critical Molecule That Links Cancer Metabolism to Redox Signaling. *Mol. Ther.* **2020**, *28*, 2358–2366. [CrossRef] [PubMed]

27. Liu, M.-R.; Zhu, W.-T.; Pei, D.-S. System Xc-: A Key Regulatory Target of Ferroptosis in Cancer. *Investig. New Drugs* **2021**, *39*, 1123–1131. [CrossRef] [PubMed]

28. Singer, E.; Judkins, J.; Salomonis, N.; Matlaf, L.; Soteropoulos, P.; McAllister, S.; Soroceanu, L. Reactive Oxygen Species-Mediated Therapeutic Response and Resistance in Glioblastoma. *Cell Death Dis.* **2015**, *6*, e1601. [CrossRef]

29. Dixon, S.J.; Lemberg, K.M.; Lamprecht, M.R.; Skouta, R.; Zaitsev, E.M.; Gleason, C.E.; Patel, D.N.; Bauer, A.J.; Cantley, A.M.; Yang, W.S.; et al. Ferroptosis: An Iron-Dependent Form of Nonapoptotic Cell Death. *Cell* **2012**, *149*, 1060–1072. [CrossRef]

30. Jiang, X.; Stockwell, B.R.; Conrad, M. Ferroptosis: Mechanisms, Biology and Role in Disease. *Nat. Rev. Mol. Cell Biol.* **2021**, *22*, 266–282. [CrossRef]

31. Dixon, S.J.; Patel, D.N.; Welsch, M.; Skouta, R.; Lee, E.D.; Hayano, M.; Thomas, A.G.; Gleason, C.E.; Tatonetti, N.P.; Slusher, B.S.; et al. Pharmacological Inhibition of Cystine–glutamate Exchange Induces Endoplasmic Reticulum Stress and Ferroptosis. *eLife* **2014**, *3*, e02523. [CrossRef] [PubMed]

32. Yamaguchi, I.; Yoshimura, S.H.; Katoh, H. High Cell Density Increases Glioblastoma Cell Viability under Glucose Deprivation via Degradation of the Cystine/glutamate Transporter xCT (SLC7A11). *J. Biol. Chem.* **2020**, *295*, 6936–6945. [CrossRef] [PubMed]

33. Ma, L.; Zhang, X.; Yu, K.; Xu, X.; Chen, T.; Shi, Y.; Wang, Y.; Qiu, S.; Guo, S.; Cui, J.; et al. Targeting SLC3A2 Subunit of System XC-Is Essential for m6A Reader YTHDC2 to Be an Endogenous Ferroptosis Inducer in Lung Adenocarcinoma. *Free Radic. Biol. Med.* **2021**, *168*, 25–43. [CrossRef] [PubMed]

34. Console, L.; Scalise, M.; Salerno, S.; Scanga, R.; Giudice, D.; De Bartolo, L.; Tonazzi, A.; Indiveri, C. N-Glycosylation Is Crucial for Trafficking and Stability of SLC3A2 (CD98). *Sci. Rep.* **2022**, *12*, 14570. [CrossRef] [PubMed]

35. Hasegawa, K.; Ikeda, S.; Yaga, M.; Watanabe, K.; Urakawa, R.; Iehara, A.; Iwai, M.; Hashiguchi, S.; Morimoto, S.; Fujiki, F.; et al. Selective Targeting of Multiple Myeloma Cells with a Monoclonal Antibody Recognizing the Ubiquitous Protein CD98 Heavy Chain. *Sci. Transl. Med.* **2022**, *14*, eaax7706. [CrossRef] [PubMed]

36. Cavada, B.S.; de Oliveira, M.V.; Osterne, V.J.S.; Pinto-Junior, V.R.; Martins, F.W.V.; Correia-Neto, C.; Pinheiro, R.F.; Leal, R.B.; Nascimento, K.S. Recent Advances in the Use of Legume Lectins for the Diagnosis and Treatment of Breast Cancer. *Biochimie* **2023**, *208*, 100–116. [CrossRef] [PubMed]

37. Stockwell, B.R.; Jiang, X. The Chemistry and Biology of Ferroptosis. *Cell Chem. Biol.* **2020**, *27*, 365–375. [CrossRef] [PubMed]

38. Mosmann, T. Rapid Colorimetric Assay for Cellular Growth and Survival: Application to Proliferation and Cytotoxicity Assays. *J. Immunol. Methods* **1983**, *65*, 55–63. [CrossRef] [PubMed]

39. Ellman, G.L. Tissue Sulfhydryl Groups. *Arch. Biochem. Biophys.* **1959**, *82*, 70–77. [CrossRef]

40. Powlesland, A.S.; Hitchen, P.G.; Parry, S.; Graham, S.A.; Barrio, M.M.; Elola, M.T.; Mordoh, J.; Dell, A.; Drickamer, K.; Taylor, M.E. Targeted Glycoproteomic Identification of Cancer Cell Glycosylation. *Glycobiology* **2009**, *19*, 899–909. [CrossRef]

41. Kirschner, K.N.; Yongye, A.B.; Tschampel, S.M.; González-Outeiriño, J.; Daniels, C.R.; Foley, B.L.; Woods, R.J. GLYCAM06: A Generalizable Biomolecular Force Field. Carbohydrates. *J. Comput. Chem.* **2008**, *29*, 622–655. [CrossRef] [PubMed]

42. Sanz-Aparicio, J.; Hermoso, J.; Grangeiro, T.B.; Calvete, J.J.; Cavada, B.S. The Crystal Structure of Canavalia Brasiliensis Lectin Suggests a Correlation between Its Quaternary Conformation and Its Distinct Biological Properties from Concanavalin A. *FEBS Lett.* **1997**, *405*, 114–118. [CrossRef] [PubMed]

43. Korb, O.; Stützle, T.; Exner, T.E. Empirical Scoring Functions for Advanced Protein-Ligand Docking with PLANTS. *J. Chem. Inf. Model.* **2009**, *49*, 84–96. [CrossRef] [PubMed]

44. Xavier, M.M.; Heck, G.S.; de Avila, M.B.; Levin, N.M.B.; Pintro, V.O.; Carvalho, N.L.; Azevedo, W.F. de SAnDReS a Computational Tool for Statistical Analysis of Docking Results and Development of Scoring Functions. *Comb. Chem. High. Throughput Screen.* **2016**, *19*, 801–812. [CrossRef] [PubMed]

45. Schneidman-Duhovny, D.; Inbar, Y.; Nussinov, R.; Wolfson, H.J. PatchDock and SymmDock: Servers for Rigid and Symmetric Docking. *Nucleic Acids Res.* **2005**, *33*, W363–W367. [CrossRef] [PubMed]

46. Jo, S.; Kim, T.; Iyer, V.G.; Im, W. CHARMM-GUI: A Web-Based Graphical User Interface for CHARMM. *J. Comput. Chem.* **2008**, *29*, 1859–1865. [CrossRef] [PubMed]

47. Lee, J.; Hitzenberger, M.; Rieger, M.; Kern, N.R.; Zacharias, M.; Im, W. CHARMM-GUI Supports the Amber Force Fields. *J. Chem. Phys.* **2020**, *153*, 035103. [CrossRef] [PubMed]

48. Tian, C.; Kasavajhala, K.; Belfon, K.A.A.; Raguette, L.; Huang, H.; Migues, A.N.; Bickel, J.; Wang, Y.; Pincay, J.; Wu, Q.; et al. ff19SB: Amino-Acid-Specific Protein Backbone Parameters Trained against Quantum Mechanics Energy Surfaces in Solution. *J. Chem. Theory Comput.* **2020**, *16*, 528–552. [CrossRef] [PubMed]

49. Klauda, J.B.; Venable, R.M.; Freites, J.A.; O'Connor, J.W.; Tobias, D.J.; Mondragon-Ramirez, C.; Vorobyov, I.; MacKerell, A.D., Jr.; Pastor, R.W. Update of the CHARMM All-Atom Additive Force Field for Lipids: Validation on Six Lipid Types. *J. Phys. Chem. B* **2010**, *114*, 7830–7843. [CrossRef]

50. Loncharich, R.J.; Brooks, B.R.; Pastor, R.W. Langevin Dynamics of Peptides: The Frictional Dependence of Isomerization Rates of N-Acetylalanyl-N′-Methylamide. *Biopolymers* **1992**, *32*, 523–535. [CrossRef]

51. Berendsen, H.J.C.; Postma, J.P.M.; van Gunsteren, W.F.; DiNola, A.; Haak, J.R. Molecular Dynamics with Coupling to an External Bath. *J. Chem. Phys.* **1984**, *81*, 3684–3690. [CrossRef]

52. Kräutler, V.; van Gunsteren, W.F.; Hünenberger, P.H. A Fast SHAKE Algorithm to Solve Distance Constraint Equations for Small Molecules in Molecular Dynamics Simulations. *J. Comput. Chem.* **2001**, *22*, 501–508. [CrossRef]

53. Essmann, U.; Perera, L.; Berkowitz, M.L.; Darden, T.; Lee, H.; Pedersen, L.G. A Smooth Particle Mesh Ewald Method. *J. Chem. Phys.* **1995**, *103*, 8577–8593. [CrossRef]

54. Roe, D.R.; Cheatham, T.E., 3rd. PTRAJ and CPPTRAJ: Software for Processing and Analysis of Molecular Dynamics Trajectory Data. *J. Chem. Theory Comput.* **2013**, *9*, 3084–3095. [CrossRef] [PubMed]

55. Stourac, J.; Vavra, O.; Kokkonen, P.; Filipovic, J.; Pinto, G.; Brezovsky, J.; Damborsky, J.; Bednar, D. Caver Web 1.0: Identification of Tunnels and Channels in Proteins and Analysis of Ligand Transport. *Nucleic Acids Res.* **2019**, *47*, W414–W422. [CrossRef] [PubMed]

56. Duhovny, D.; Nussinov, R.; Wolfson, H.J. Efficient Unbound Docking of Rigid Molecules. In *Algorithms in Bioinformatics*; Springer: Berlin/Heidelberg, Germany, 2002; pp. 185–200.

57. Pratt, J.; Roy, R.; Annabi, B. Concanavalin-A-Induced Autophagy Biomarkers Requires Membrane Type-1 Matrix Metalloproteinase Intracellular Signaling in Glioblastoma Cells. *Glycobiology* **2012**, *22*, 1245–1255. [CrossRef] [PubMed]

58. Yamamoto, M.; Mohanam, S.; Sawaya, R.; Fuller, G.N.; Seiki, M.; Sato, H.; Gokaslan, Z.L.; Liotta, L.A.; Nicolson, G.L.; Rao, J.S. Differential Expression of Membrane-Type Matrix Metalloproteinase and Its Correlation with Gelatinase A Activation in Human Malignant Brain Tumors In Vivo and In Vitro. *Cancer Res.* **1996**, *56*, 384–392. [PubMed]

59. Osterne, V.J.S.; Pinto-Junior, V.R.; Oliveira, M.V.; Nascimento, K.S.; Van Damme, E.J.M.; Cavada, B.S. Computational Insights into the Circular Permutation Roles on ConA Binding and Structural Stability. *Curr. Res. Struct. Biol.* **2024**, *7*, 100140. [CrossRef] [PubMed]

60. Cavada, B.S.; Osterne, V.J.S.; Lossio, C.F.; Pinto-Junior, V.R.; Oliveira, M.V.; Silva, M.T.L.; Leal, R.B.; Nascimento, K.S. One Century of ConA and 40 Years of ConBr Research: A Structural Review. *Int. J. Biol. Macromol.* **2019**, *134*, 901–911. [CrossRef] [PubMed]

61. Polewski, M.D.; Reveron-Thornton, R.F.; Cherryholmes, G.A.; Marinov, G.K.; Cassady, K.; Aboody, K.S. Increased Expression of System Xc- in Glioblastoma Confers an Altered Metabolic State and Temozolomide Resistance. *Mol. Cancer Res.* **2016**, *14*, 1229–1242. [CrossRef]

62. An, S.; Lu, X.; Zhao, W.; Sun, T.; Zhang, Y.; Lu, Y.; Jiang, C. Amino Acid Metabolism Abnormity and Microenvironment Variation Mediated Targeting and Controlled Glioma Chemotherapy. *Small* **2016**, *12*, 5633–5645. [CrossRef] [PubMed]

63. Chew, K.S.; Wells, R.C.; Moshkforoush, A.; Chan, D.; Lechtenberg, K.J.; Tran, H.L.; Chow, J.; Kim, D.J.; Robles-Colmenares, Y.; Srivastava, D.B.; et al. CD98hc Is a Target for Brain Delivery of Biotherapeutics. *Nat. Commun.* **2023**, *14*, 5053. [CrossRef] [PubMed]

64. Dixon, S.J.; Stockwell, B.R. The Hallmarks of Ferroptosis. *Annu. Rev. Cancer Biol.* **2019**, *3*, 35–54. [CrossRef]

65. Kar, F.; Kacar, S.; Hacioglu, C.; Kanbak, G.; Sahinturk, V. Concanavalin A Induces Apoptosis in a Dose-Dependent Manner by Modulating Thiol/disulfide Homeostasis in C6 Glioblastoma Cells. *J. Biochem. Mol. Toxicol.* **2021**, *35*, e22742. [CrossRef] [PubMed]

66. Zeng, T.; Deng, G.; Zhong, W.; Gao, Z.; Ma, S.; Mo, C.; Li, Y.; Huang, S.; Zhou, C.; Lai, Y.; et al. Indoleamine 2, 3-Dioxygenase 1enhanceshepatocytes Ferroptosis in Acute Immune Hepatitis Associated with Excess Nitrative Stress. *Free Radic. Biol. Med.* **2020**, *152*, 668–679. [CrossRef]

67. Yan, B.; Ai, Y.; Sun, Q.; Ma, Y.; Cao, Y.; Wang, J.; Zhang, Z.; Wang, X. Membrane Damage during Ferroptosis Is Caused by Oxidation of Phospholipids Catalyzed by the Oxidoreductases POR and CYB5R1. *Mol. Cell* **2021**, *81*, 355–369.e10. [CrossRef]